Spectral and Spatial Energetics of the GISS Model Atmosphere

J. TENENBAUM

Institute for Space Studies, Goddard Space Flight Center, NASA, New York, N. Y. 10025
and State University of New York, College at Purchase 10577

(Manuscript received 18 April 1975, in revised form 28 August 1975)

ABSTRACT

A calculation of the spectral and spatial energetics of the Goddard Institute for Space Studies (GISS) 9-level model of the global atmosphere is given. Results are presented from a model simulation of January 1973 and compared with previous model studies and an observational analysis for the Northern Hemisphere. The spectral analysis permits detailed study of those physical processes of scale larger than the grid spacing and allows indirect conclusions concerning unresolved subgrid-scale processes. For larger-than-grid-scale processes we conclude that: 1) the GISS model with a relatively coarse resolution of 4° latitude by 5° longitude produces significant nonlinear energy transfers; 2) baroclinic conversion is large near planetary wavenumber 6, but both the GISS model and another orographic model show a less peaked structure than non-orographic models and observations; and 3) Saltzman's previously published compilation of observed spectral energetics is based on analyses that, when normalized, are probably too large by about 25%. A linear fit to the kinetic energy spectrum yields a power law of −2.6 in the wavenumber region 8 to 15. For subgrid-scale processes, the turbulence theory result of very small energy flux cascade is obtained. For the spatial energetics we find good agreement with recently published climatological data.

1. Introduction

A description and numerical results for the Goddard Institute for Space Studies (GISS) global atmospheric model have recently been published (Somerville *et al.*, 1974). In this paper we extend these results by presenting a detailed spectral and spatial analysis of the GISS model energetics for January 1973. The model spectral analyses are compared with the results of identical calculations performed on observational data for January 1973, with analyses of other general circulation models (Manabe *et al.*, 1970), and with observational data reviewed by Saltzman (1970). The spatial analyses are compared with recent observational results of Peixoto and Oort (1974) and Oort and Peixoto (1974).

Although the model calculations are over a global domain, only Northern Hemisphere results will be presented. The Southern Hemisphere results lack sufficient observational data for comparison. We will deal with most phenomena which are of interest using spectral techniques with the exception of tropical waves. This is a large area of study in its own right (Wallace, 1971). In this paper, our primary purpose is to compare the model energetics with observation in the spectral domain and to document the model energetics in the spatial domain..

The standard energy diagram contains components for zonal available potential energy, eddy available potential energy, zonal kinetic energy and eddy kinetic energy, and conversions among these four components (Lorenz, 1967). The GISS model is in basic agreement with Oort's (1964) calculation of these quantities from observational data (Somerville *et al.*, 1974). Further insight into the model's strengths and weaknesses is provided by obtaining a spectral decomposition. The technique involves subdividing the eddy components and conversions into their Fourier transform components around latitude circles.

The results from such a decomposition provide insight into two related areas. First, we may verify the behavior of physical processes explicitly resolved by the model. An example is large-scale baroclinic conversion in the production of mid-latitude cyclones. These results will be discussed under the heading of "larger-than-grid-scale processes." Second, we may draw indirect concludions about subgrid-scale processes. No finite grid model can explicitly account for turbulent motions on a scale smaller than the grid spacing. Implicit assumptions must be made concerning the subgrid-scale energy and its interaction with the larger scales. These assumptions reflect our solution to the "closure problem" of turbulence theory.

The GISS model is described completely in Somerville *et al.* (1974), which will hereafter be referred to as S. The major characteristics are as follows. It is a 9-level, primitive equation model in σ-coordinates. The domain is global with a 4° latitude by 5° longitude grid. The model includes orography, an extensive hydrological cycle, and parameterized subgrid-scale cumu-

TABLE 1. Definitions of energies and conversions used in this paper, Saltzman (1970), and Manabe *et al.* (1970).

This paper	Definition	Saltzman (1970)	Manabe *et al.* (1970)[a]
$K(0)$	zonal kinetic energy	$K(0)$	K_Z
$P(0)$	zonal available potential energy	$P(0)$	P_Z
$K(n)$	eddy kinetic energy of wavenumber n	$K(n)$	K_n
$P(n)$	eddy available potential energy of wavenumber n	$P(n)$	—
$C[P(0),P(n)]$	conversion from $P(0)$ to $P(n)$	$R(n)$	—
$C[P(n),K(n)]$	conversion from $P(n)$ to $K(n)$	$C(n)$	P_n
$C[K(n),K(0)]$	conversion from $K(n)$ to $K(0)$	$M(n)$	T_n
$C[K(m\|n)]$	conversion $K(m)$ to $K(n)$ summed from $m=1$ to a maximum value, M	$L(n)$	
$D(0)$	dissipation from zonal kinetic energy	$D(0)$	$D(0)$
$D(n)$	dissipation from eddy kinetic energy of wavenumber n	$D(n)$	$D(n)$
$E(n)$	enstrophy of wavenumber n	—	—

[a] Manabe *et al.*'s T_n is the sum of $C[K(n),K(0)]$ and $C[K(m|n)]$.

lus convection. The radiation calculations take into account the calculated cloud and water vapor distribution. A quasi-conservative spatial differencing scheme due to Arakawa (1966, 1970, 1972) is used with a 5 min time step.

In the next section we will review the theory and results of previous spectral studies. Section 3 presents the detailed methods used in this study. In Section 4 we present our results and in Section 5 we discuss our conclusions.

2. Theory and previous studies

a. Spectral energetics

The procedures for spectral analysis of the equations of motion were given by Saltzman (1957). He argued that most turbulence theory analyses dealt with the growth of eddies at the expense of the mean flow. By contrast, direct conversion from eddy available potential energy to eddy kinetic energy is meteorologically significant. The result is a growth of the mean flow at the expense of the eddies. Saltzman concluded that a detailed spectral analysis of the equations of motion would allow both directions of energy flow to be examined together.

A number of studies, following Saltzman's suggestion, attempted to extract portions of the spectral energy cycle from the observational data. These efforts were reviewed by Saltzman (1970) where he also gives the integrals used to calculate the spectral energies and conversions. His nomenclature differs from that of nonspectral energetics papers. Table 1 gives the definition of each spectral energy and conversion and the translation between the nomenclature used in Saltzman (1970), Manabe *et al.* (1970), and this paper. Table 2 defines all other symbols used in this paper. Saltzman combined the most comprehensive of the observational papers (Yang, 1967; Wiin-Nielsen, 1964; Saltzman and Fleisher, 1961) to obtain the overall spectral energy diagram for winter shown in Fig. 1.

The results imply a cycle consisting of diabatic generation of zonal available potential energy, $P(0)$, followed by a cascading down to the various wavenumber components of eddy available potential energy, $P(n)$, with most energy left in the smaller wavenumbers n. Baroclinic conversion then occurs to eddy kinetic energy, $K(n)$, with the maximum occurring at $n=6$ corresponding to the wavelength of maximum baroclinic instability (Kuo, 1952). Finally, the individual eddies feed $K(0)$, the energy of the zonal motion. This overall process is consistent with the total energy

TABLE 2. Symbols used in this paper.

n	wavenumber
M	cutoff in summation of $C[K(m\|n)]\equiv \sum_{m=1}^{M} C[K(m),K(n)]$, where $C[K(m),K(n)]$ is the conversion from $K(m)$ to $K(n)$
λ	latitude
ϕ	longitude
p	pressure
t	time
a	radius of earth
u	zonal velocity
v	meridional velocity
$v(n)$	(complex) Fourier transform of meridional velocity v
$[x]$	zonal average $\left[=\frac{1}{2\pi}\int_0^{2\pi} x\,d\lambda\right]$
ω	pressure velocity dp/dt
σ_x	variance of variable $x \left[=\frac{1}{2\pi}\int_0^{2\pi} d\lambda(x-[x])^2\right]^{\frac{1}{2}}$
n_c	cutoff wavenumber in summation of nonlinear interaction term: see Table 3
$\Delta(n)$	residual in $K(n)$ $\{=C[P(n),K(n)]+C[K(m\|n)]-C[K(n),K(0)]-D(n)\}$
$F(n)$	energy flux through wavenumber n $\left[=\int_0^n dn' C[k(m\|n')]\right]$

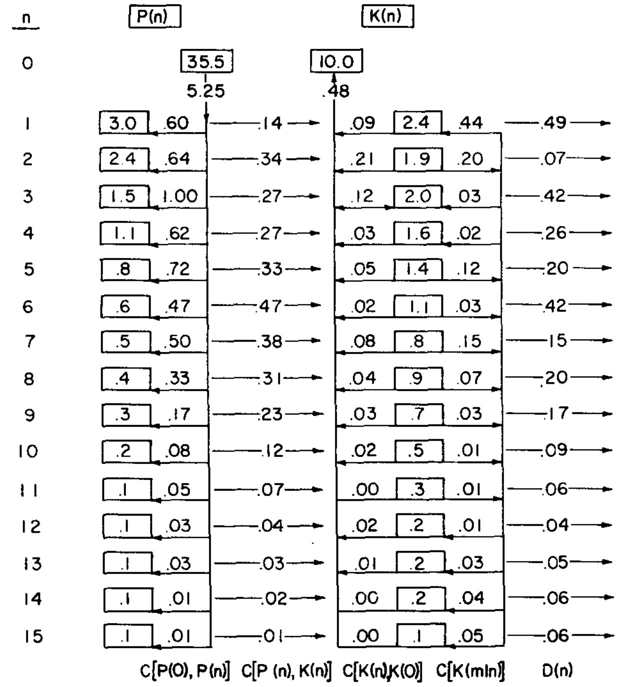

FIG. 1. Spectral energy diagram for winter from Saltzman (1970). Boxes contain zonal energies, $P(0)$ and $K(0)$, and eddy energies, $P(n)$ and $K(n)$, associated with wavenumbers 1 to 15. Units for energies are 10^5 J m^{-2}. Labelled arrows are conversions with the symbol for each conversion given at the bottom of each column. Units for conversions are W m^{-2}.

flow (Oort, 1964) and with the view of meteorological phenomena as negative viscosity effects (Starr, 1968). The correspondence of the model and observational energy cycles measures how well the model incorporates the larger-than-grid-scale features of the equations of motion.

Subgrid-scale phenomena are analyzed in terms of the functional dependence on wavenumber of $K(n)$ and $P(n)$. Two classes of theories have been suggested in the literature. The first treats atmospheric motions as predominantly two-dimensional. The absence of vortex tube stretching in two-dimensional flow produces two quadratic integrals to be conserved, energy and enstrophy (equal to $\frac{1}{2}$ the mean square vorticity). For wavenumbers from 8 to 15 a simple power law dependence may be derived using dimensional analysis and assuming no generative or dissipative processes in this wavenumber region (Kraichnan, 1967; Leith, 1968). If, in addition, a constant enstrophy cascade is assumed one obtains a -3 power law, while a constant energy cascade leads to a $-5/3$ power law, equivalent to the Kolmogoroff analysis of classical turbulence theory.

The second class of theory has been suggested by Charney (1971). He argues that the turbulent behavior of the atmosphere is inherently not two-dimensional as is clear from the nature of baroclinicity itself. By an elegant analysis he is able to show, however, that a three-dimensional quasi-geostrophic theory also leads to the same power law dependences. He additionally derives predictions on the equipartition of spectral kinetic energy in the zonal and meridional directions.

Studies of observational and model data have confirmed that the -3 power law holds approximately for the region of wavenumbers 8–15. (Wiin-Nielsen, 1967; Manabe *et al.*, 1970; Wellck *et al.*, 1971). The objections raised by Wiin-Nielsen (1967), however, have not always been considered. He argues that, when the effect of filtering implicit in the transformation to uniform grids is included, the real atmospheric slope has a -2.5 power law. More recently, Julian and Cline (1974) have examined the untransformed observational data for kinetic energy at a single latitude, 52°N. Their winter results for the power law slope are -2.5, -2.7 and -2.8 for 850, 500 and 250 mb, respectively.

Additional turbulence theory effects can be examined in general circulation models. The power law behavior can be checked directly. Also, the assumption that the power law regions are removed from generative and dissipative regions (and that constant enstrophy cascade occurs) requires that zero energy flux should cascade through these regions. Whether analagous behavior occurs for general circulation models can be checked by examining the conversion flux, $C[K(n), K(0)]$, which is defined as the conversion from $K(n)$ to $K(0)$.

The major published general circulation models are those from the Geophysical Fluid Dynamics Laboratory [GFDL] (Smagorinsky *et al.*, 1965; Manabe *et al.*, 1965, 1970; Manabe and Terpstra, 1974) and the National Center for Atmospheric Research [NCAR] (Kasahara and Washington, 1967, 1971; Wellck *et al.*, 1971; and data in Charney, 1971). A number of studies have been made with each model. The overall spectra appeared in papers devoted to examining the effects of horizontal resolution (GFDL, Manabe *et al.*, 1970; and NCAR, Wellck *et al.*, 1971) with some additional GFDL results in Manabe and Terpstra (1974). The GFDL results include spectra of eddy kinetic energy and related conversions. Manabe *et al.* conclude that decreasing the grid size substantially increased the nonlinear conversion effects in the baroclinic wavenumber region less than wavenumber 6. The results from the NCAR study (Wellck *et al.*, 1971) are limited to $K(n)$ only but imply similar conclusions.

b. Spatial energetics

Non-spectral studies which deal with sums over all n were suggested by Lorenz (1955, 1967). Observational results were presented by Oort (1964). Paper S presented an energy diagram in general agreement with Oort's 1964 results. Since that time Peixoto and Oort (1974) and Oort and Peixoto (1974) have presented data for individual months and given explicit results for the spatial dependence on latitude and height. Both

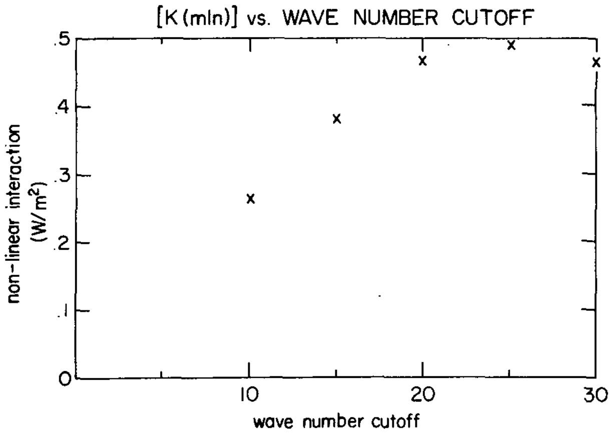

FIG. 2. The nonlinear interaction term, $C[K(m|n)]$, as a function of the wavenumber cutoff used in its calculation.

their results for $P(0)$ and our method of calculation of the static stability coefficient differ significantly from those of Oort (1964) and Paper S, respectively. The new papers of Oort and Peixoto also contain data on the spatial distribution of the energies and conversions which permit a more detailed test of the model.

3. Methods

Spectral analyses of atmospheric data can be performed in one, two, or three dimensions. In part the choice depends on assumptions concerning the dimensionality of the turbulent processes. For two-dimensional turbulence theories and a spherical geometry, Baer (1972) has used spherical harmonics rather than the more common one-dimensional Fourier transform around latitude circles. His reasons are twofold: first, to avoid aliasing by oblique nonzonal waves, and second, to allow use of the exact conservation properties of two-dimensional turbulence theories. Lilly (1972) presents similar arguments, especially for analyses using rectangular geometries.

For the present study, two-dimensional analyses present both theoretical and practical problems. Baer's techniques require the use of global data or the assumption of some symmetry about the equator. As a result our Northern Hemisphere results would be partially dependent on Southern Hemisphere calculations. Less fundamentally, comprehensive observational data, other models, and Saltzman's results are available only in one-dimensional form. Since our primary purpose is to present a comparison of the GISS model with the atmosphere, with other models, and with Saltzman's extended energetics diagram, we have performed only one-dimensional analyses.

The global domain of the GISS model eliminates the need for artificial boundary conditions at the equator. In forming the Northern Hemisphere energetics, one must allow for transfers across the equator. Oort and Peixoto (1974) have calculated these transfers and shown that the only major contribution for January is an increase of $P(0)$. Our conclusions are limited to results of conversions to and from $K(0)$ and $K(n)$.

The nonlinear interaction term

$$C[K(m|n)]\equiv \sum_{m=1}^{M} C[K(m),K(n)]$$

requires an arbitrary cutoff of some value M. Fig. 2 shows the value of this term as a function of M. Values of M greater than 25 appear adequate. The results presented in Section 4 use $M=30$, the maximum wavenumber calculated in our analysis.

Our Fourier transform pairs are defined identically to those of Saltzman (1970):

$$g(\lambda,\phi,p,t)=\sum_{n=-\infty}^{\infty} G(n,\phi,p,t)e^{in\lambda},$$

$$G(n,\phi,p,t)=\frac{1}{2\pi}\int_0^{2\pi} g(\lambda,\phi,p,t)e^{-in\lambda}d\lambda,$$

where g is an arbitrary function of longitude λ, latitude ϕ, pressure p, and time t; G is its Fourier transform, a function of wavenumber n. The actual transformations are done by the fast-Fourier-transform method (Cooley and Tukey, 1965). The formula for each energy and conversion are those given in Saltzman (1970). We have also calculated enstrophy which is given by

$$E(n)=\left|\frac{1}{a\cos\phi}inv(n)-\frac{1}{a}\frac{\partial u(n)}{\partial\phi}\right|^2,$$

where $E(n)$ is the enstrophy transform, a is the earth's radius, and $u(n)$ and $v(n)$ are the (complex) transforms of the velocities.

During the model runs, all basic variables were saved at intervals of 2 h of simulated time. The climatological results given in S present time averages of the appropriate variables at 12 h intervals during January 1973. The spectral results in this paper represent time averages of the spectral quantities evaluated at 12 h intervals for January 1973. For comparison purposes, the spectral results were calculated both for the model and for a National Meteorological Center (NMC) observational analysis (Shuman and Hovermale, 1968) experimentally extended south of 18°N (Flattery, 1971). Unless otherwise indicated the domain of comparison is the entire Northern Hemisphere below 110 mb.

A calculational problem arises in the treatment of Fourier transformations in the presence of orography. Except for the most recent GFDL study (Manabe and Terpstra, 1974) orography was suppressed in the previous GFDL and NCAR studies that contain spectral results (Manabe *et al.*, 1970; Wellck *et al.*, 1971). Most observational data used by Saltzman in Fig. 1 have relatively coarse vertical resolution (data at 850 mb, 700 mb, . . .) near the ground. Although the

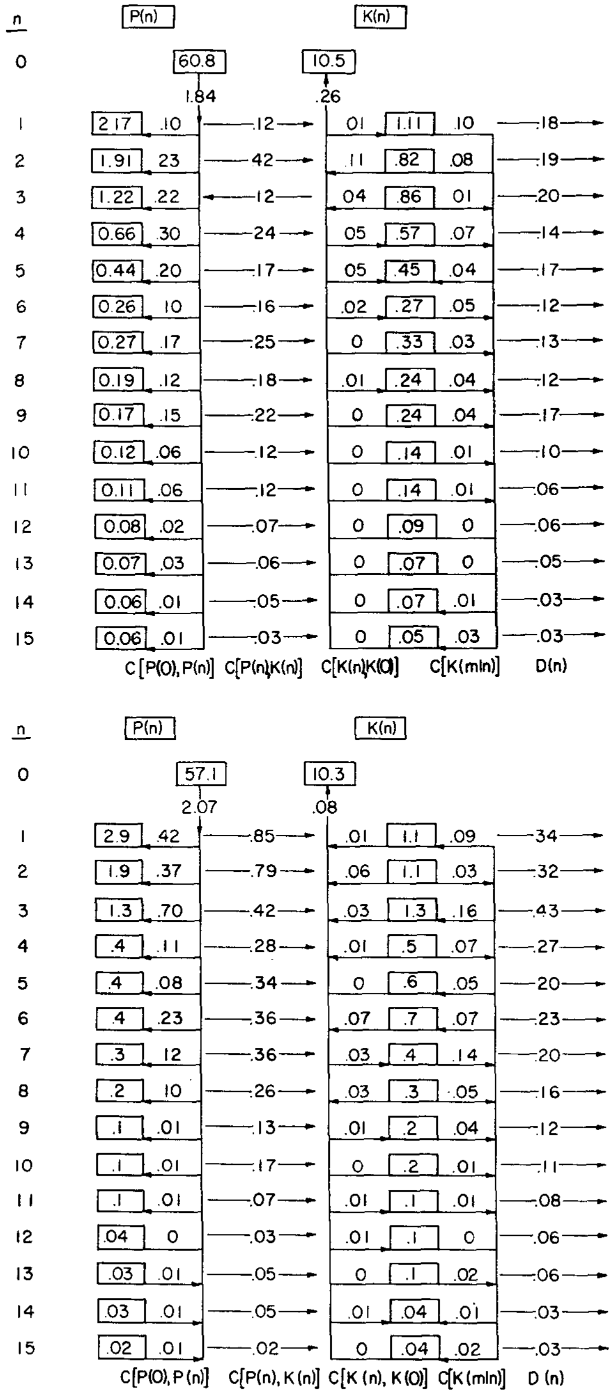

FIG. 3. (a) Spectral energy diagram for January 1973 as calculated from the GISS model. (b) Spectral energy diagram for January 1973 as calculated from NMC observations. Boxes contain zonal energies, $P(0)$ and $K(0)$, and eddy energies, $P(n)$ and $K(n)$, associated with wavenumbers 1 to 15. Units for energies are 10^5 J m^{-2}. Labelled arrows are conversions with the symbol for each conversion given at the bottom of each column. Units for conversions are W m^{-2}.

GISS model uses σ-coordinates, the comparisons with observational data in this paper and S are made in pressure coordinates. Furthermore, the physical interpretation of waves on σ-surfaces is not obvious.

Once the choice of pressure-coordinate comparisons is made, one must face the issue of what to do about those pressure surfaces which intercept the earth's surface. The problem is closely related to the incomplete circle effect studied by Baer (1973) and the non-uniform station spacing effect studied by Julian and Cline (1974). Two classes of meteorological variables must be distinguished. First, variables such as u, the zonal wind, satisfy the relation $[u]-\sigma_u<0<[u]+\sigma_u$ where $[u]$ is the zonal average and σ_u the variance around a latitude circle. Here the inclusion of the subsurface points either as 0 or as $[u]$ does not drastically affect spectral results. Specifically, $K(1)$ changed by only 4% between these two choices. The results presented in this paper were obtained using the choice of 0 for such variables.

A variable such as T presents a different problem. Clearly the inequality

$$[T]-\sigma_T<0<[T]+\sigma_T$$

is not satisfied. In this case, the choice was made of substituting $[T]$ for such variables. Such a choice is not bias free in the sense of not altering the various wavenumber components. Appendix A shows the problem in more detail and gives the exact bias-free solution. Such a solution would be extremely time consuming and in view of small effects was not adopted. It is important to realize that the resulting choice is arbitrary, and, as a result, one cannot attach significance of more than a few percent to results and fitted slopes.

4. Results of standard GISS model

a. *Larger-than-grid-scale*

Fig. 3 presents the spectral energetics diagram corresponding to Fig. 1 for January 1973 as calculated from the model (a) and as calculated from the NMC observational analysis (b). The $K(0)$, $P(0)$ and $P(n)$ terms display approximate agreement between model and observations. The conversions $C[P(n), K(n)]$ are very difficult to calculate accurately due to the dependence on ω, the vertical pressure velocity. This field is calculated from mass convergence in our analysis while the data used by Saltzman assumes a quasi-geostrophic relationship. The conversions show very large fluctuations in the orographic region, wavenumbers $\sim$1–5. Fig. 4 shows this conversion for wavenumbers 4–15 in graphical form. There is a difference in shape between the somewhat peaked observations (Saltzman and NMC) and the more broadened GISS and GFDL models. The increased peaking also occurred in the GFDL model in the absence of orography (Manabe and Terpstra, 1974, Fig. 8.3). Note that their results are limited to the latitude band 40–50°N. We conclude that there is a definite difference in the shape of the spectrum between models and

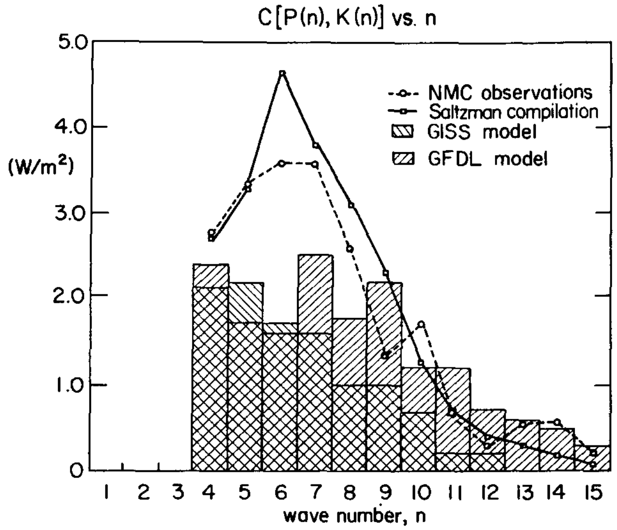

FIG. 4. The conversion from eddy available potential energy to eddy kinetic energy, $C[P(n), K(n)]$, vs wavenumber. Wavenumbers 1 through 3 are not comparable due to differing treatments of orography and fluctuate substantially. Their numerical values are given in Figs. 1 and 3. Saltzman compilation from Saltzman (1970). GFDL model from Manabe *et al.* (1970).

observations. Whether the effect is due to basic difficulties with ω-dependent quantities or to more consistent treatment of orography in the models requires further investigation. Note that the original data used by Saltzman were limited to one level.

Comprehensive spectral data for the other conversions have been presented in only two places: Saltzman summarizes Yang's (1967) results for $C[K(n), K(0)]$ and $C[K(m|n)]$, and Manabe *et al.* (1970) present $C[P(n), K(n)]$ for the GFDL model. The Manabe *et al.* results labelled T_n are not directly comparable with Yang's results. Specifically, Manabe *et al.*'s T_n is really the sum of $C[K(m|n)]$ and $C[K(n), K(0)]$. They do not present the results separately.

Manabe *et al.* argue that the nonlinear interaction term $C[K(m|n)]+C[K(n), K(0)]$ was small until the resolution was changed from about 5° to 2.5°. This change is shown in Fig. 5a. Our model results are shown in Fig. 5b. Wavenumbers 1 through 5 are not comparable since Manabe *et al.* omit orography. {See Manabe and Terpstra (1974) for the effects of adding orography on the conversion $C[P(n), K(n)]$}. Table 3 shows the integrated contributions from wavenumber 15 to a cutoff wavenumber n_c. The nonlinear term is clearly significant in the GISS model independent of the arbitrary cutoff wavenumber n_c. These results indicate that the GISS model (with orography) produces nonlinear energy transfers using relatively coarse (~4°) resolution.

TABLE 3. Integrated contributions (W m⁻²) from wavenumber n_c to 15 for $C[K(n), K(0)]+C[K(m|n)]$.

Cutoff wavenumber n_c	GFDL ~5°	GFDL ~2.5°	GISS 4°	NMC 4°
6	+0.01	−0.10	−0.18	−0.18
5	−0.02	−0.21	−0.20	−0.23
4	−0.07	−0.32	−0.31	−0.32

Yang (1967) presents his results by grouping the wavenumbers to determine the conversions with somewhat higher statistical confidence. In Table 4 we have followed this procedure. Large disagreements are still present for all conversions except $C[K(m|n)]$ for wavenumbers 1 through 5. The conversion $C[P(n), K(n)]$ which depends sensitively on ω fluctuates substantially

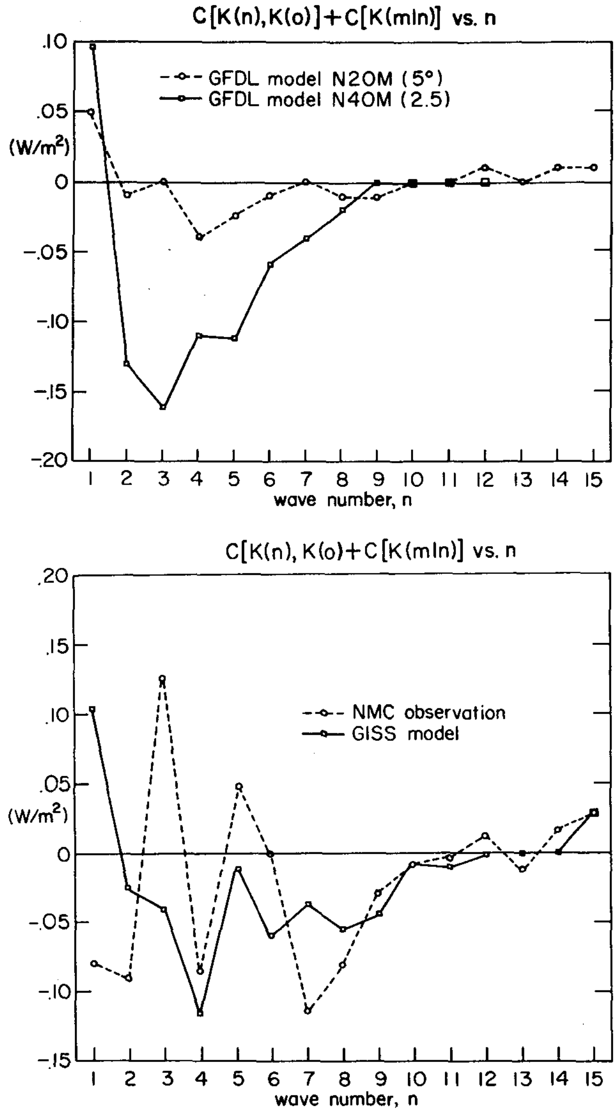

FIG. 5. The nonlinear interaction terms, $C[K(n), K(0)]+C[K(m|n)]$, vs wavenumber. (a) GFDL results from Manabe *et al.* (1970) for nominal resolutions of 5° (their case N20M) and 2.5° (N40M). (b) GISS model and NMC observations for January 1973.

TABLE 4. Conversions grouped as in Yang (1967). GFDL data are from Manabe *et al.* (1970). Units are W m⁻².

	1–5				6–10				11–15			
	GFDL	GISS	NMC	Yang	GFDL	GISS	NMC	Yang	GFDL	GISS	NMC	Yang
$C[P(0), P(n)]$	—	1.05	1.68	3.58	—	0.60	0.47	1.55	—	0.13	0.04	0.13
$C[P(n), K(n)]$	1.10	0.83	2.68	1.35	0.60	0.93	1.28	1.51	0.12	0.33	0.22	0.17
$C[K(m\|n)]$	—	0.14	0.20	0.17	—	0.17	0.17	0.29	—	0.02	0	0.15
$C[K(n), K(0)]$	—	0.24	0.10	0.26	—	0.03	0.06	0.19	—	0	0.01	0.03
$D(n)$	0.93	0.88	1.56	1.37	0.56	0.64	0.82	1.03	0.22	0.23	0.26	0.27

in all wavenumber regions. For other conversions the GISS model and NMC analysis agree in the baroclinic region ($n=6$ to 10). For $D(n)$ we also have data from the GFDL model. Fig. 6 shows that the wavenumber spectrum of both models agrees quite well, while differing in magnitude from the NMC analysis.

Examination of Figs. 1 and 3 and Table 4 indicates that in the baroclinic wavenumber region (and to some extent above it), Saltzman's compilation is based on analyses which represent a very active atmosphere. Specific examples are the energies $K(n)$, and conversions $C[K(n), K(0)]$, $C[K(m|n)]$, $C[P(0), P(n)]$, $D(n)$. These results derive from analyses of Wiin-Nielsen and Yang on data for 1962 (January, April, July, December) and February 1963 to January 1964. Peixoto and Oort (1974) have presented non-spectral data for these same years. Since interannual variation might explain the differences we have compared the $K(n)$ terms in detail in Table 5. Wiin-Nielsen's data for 1962 exceed those of Peixoto and Oort by 30%. For the month by month data each eddy kinetic energy of Yang/Wiin-Nielsen exceeds Peixoto and Oort by 20% in July and August and 25% for the rest of the year.

Because the Peixoto-Oort calculation deals more directly and comprehensively with the primary data we are inclined to accept it as more nearly correct. Consequently, we conclude that the derived spectral energies and conversions given by Saltzman are high by 25%. A later calculation (Wiin-Nielsen, 1967) from the same data was subsequently used by Leith (1971) to analyze atmospheric predictability. Leith concluded that a decrease of a factor of 4 in eddy kinetic energy would increase his time scales by a factor of 2. Thus the large magnitude of the spectral data may explain part of the unusually short predictability limit of 1 week, a possibility suggested in Leith's paper.

Several other points may be noted. We do not reproduce the anomalous flow of kinetic energy from $K(0)$ to $K(3)$ found by Yang. We do, however, find an anomalous conversion of energy from $K(3)$ to $P(3)$ in the model in opposition to the observations and Yang's data. Here again a $C[P(n), K(n)]$ proportional to ω is somewhat suspect. The flow of energy from $P(0)$ to $P(n)$ is consistent between the model and NMC data, but individual n scatter widely. We do verify Yang's result that this conversion is dominated by the low ($n<8$) wavenumbers.

Finally, unlike Saltzman's compilation we have been able to calculate all inputs and outputs to the quantity $K(n)$. His $D(n)$ must be calculated as a difference. Fig. 7 shows our residual values defined as

$$\Delta(n)=C[P(n), K(n)]+C[K(m|n)] -C[K(n), K(0)]-D(n).$$

Note that the model is in reasonable balance except for wavenumbers 2 and 3 where one expects the standing waves induced by the orography to be important (Manabe and Terpstra, 1974). We conclude that the

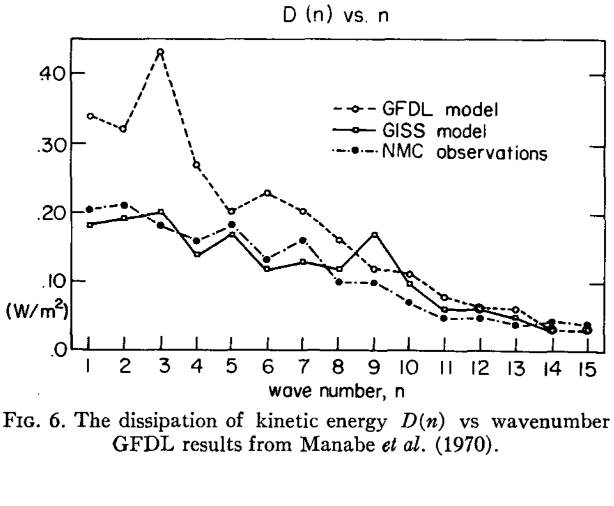

FIG. 6. The dissipation of kinetic energy $D(n)$ vs wavenumber GFDL results from Manabe *et al.* (1970).

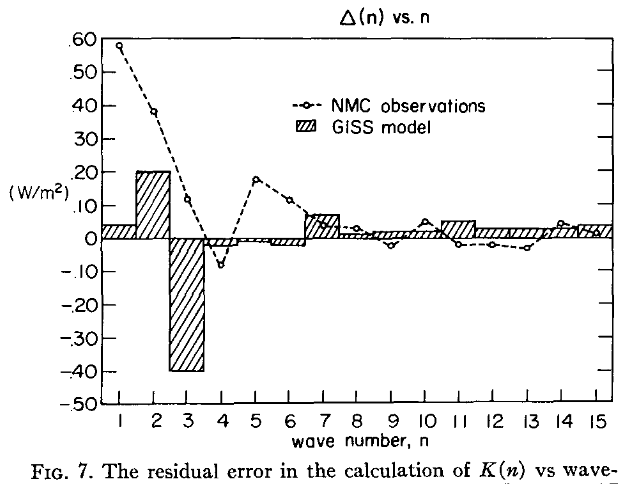

FIG. 7. The residual error in the calculation of $K(n)$ vs wavenumber. The residual is defined as $\Delta(n)=C[P(n),K(n)]+C[K(m|n)]-C[K(n),K(0)]-D(n)$.

TABLE 5. Eddy kinetic energy by months and years in units of 10^3 J m^{-2}.

Monthly			Annual		
Month	Win-Nielsen 1963[a]	Peixoto and Oort 1958–1963[e]	Years	Wiin-Nielsen[e]	Peixoto and Oort[e]
Jan.	1618[b],1673[c],1365[d]	931	1958–1959		813
Feb.	1299	870	1959–1960		793
Mar.	1224	798	1960–1961		781
Apr.	1102,1216[c]	720	1961–1962		827
May	912	645	1962	1180	
June	776	569	1962–1963		818
July	652, 685[c]	514			
Aug.	618	508			
Sept.	876	569			
Oct.	1001,1148[c]	679			
Nov.	1033	773			
Dec.	1345	863			

[a] Data for 1963 from Wiin-Nielsen (1967) except as noted.
[b] Data for 1963 from Wiin-Nielsen (1964).
[c] Data for 1962 from Wiin-Nielsen (1964).
[d] Data for 1964 from Wiin-Nielsen (1967).
[e] Data from May 1958 through April 1963 from Peixoto and Oort (1974), averaged from May through April of following year.

spectral energetics show the same precision (~20%) as the non-spectral energetics, and that there is no systematic bias as a function of wavenumber.

b. *Subgrid-scale*

The $K(n)$ and $P(n)$ spectra are the general circulation model results most directly related to turbulence theories. For 5° longitude spacing, wavenumbers out to $n=36$ are at least theoretically possible. For the observational data Julian *et al.* (1970) show that spectra are not completely trustworthy beyond $n=15$. Figs. 8a and b present the $K(n)$ and $P(n)$ spectra for the model and observational data. The fitted slopes are summarized in Table 6.

In interpreting $K(n)$, we may make the following observations. First, the GISS model has nominally twice the grid spacing of the GFDL model. Second, a linear fit between $n=8$ and 15 for the GISS data yields a -2.6 power law. Third, as discussed above, the Saltzman results are from a very energetic year. Note that while the observational data possess an apparent -3 slope, both Wiin-Nielsen (1967) and Julian and Cline (1974) have argued that such a slope may be an artifact of the transformation processes applied to observational data. As indicated above some turbulence theories yield a regime of -3 power falloff if zero energy cascade is assumed and $-5/3$ if zero enstrophy cascade is assumed. Both models and observations are clearly closer to -3 than $-5/3$ but the evidence is not clear whether the atmosphere is exactly -3. Table 6 also gives the results of two other arbitrary choices of wavenumber limits for $K(n)$. Inclusion of $n=6$ to 15 clearly takes us out of a possible inertial range and yields a slope of -2.0. Inclusion of $n=8$ to 20 changes the slope to -2.4. This gives a sense of the uncertainty in the basic result of -2.6.

TABLE 6. Summary of linear fits to the data for $K(n)$, $P(n)$ and enstrophy. Wavenumber ranges as indicated.

Variable	Source	Wave-numbers	Slope of linear fit
K	model	8–15	−2.6
	NMC	8–15	−3.6
P	model	8–15	−2.0
	NMC	8–15	−3.2
enstrophy	model	8–15	−1.0
	NMC	8–15	−2.2
K	model	6–15	−2.0
	model	8–20	−2.4
	model with 9 levels	8–15	−2.6

The $P(n)$ data show similar behavior with the GISS model having a lesser slope of -2.0 and a pronounced flattening between wavenumbers 15 and 30 which does not appear in the observational data. For a 9-level model $P(n)$ is also expected to possess a slope of -3 (Charney, 1971). Our result of -2.0 clearly differs from this value and possibly is a consequence in this region of the flattening seen at larger wavenumbers. No published results for $P(n)$ are available for other models. In both $K(n)$ and $P(n)$ the model has a less negative slope than the observational data. This effect is most likely due to excess smoothing in the NMC analysis or incorrect effective viscosity in the model. The flattening at larger wavenumbers in $P(n)$ is substantially reduced when we varied the model's eddy momentum coefficient as discussed in Section 4f.

Our results permit a check on one of the necessary conditions for the existence of an inertial subrange.

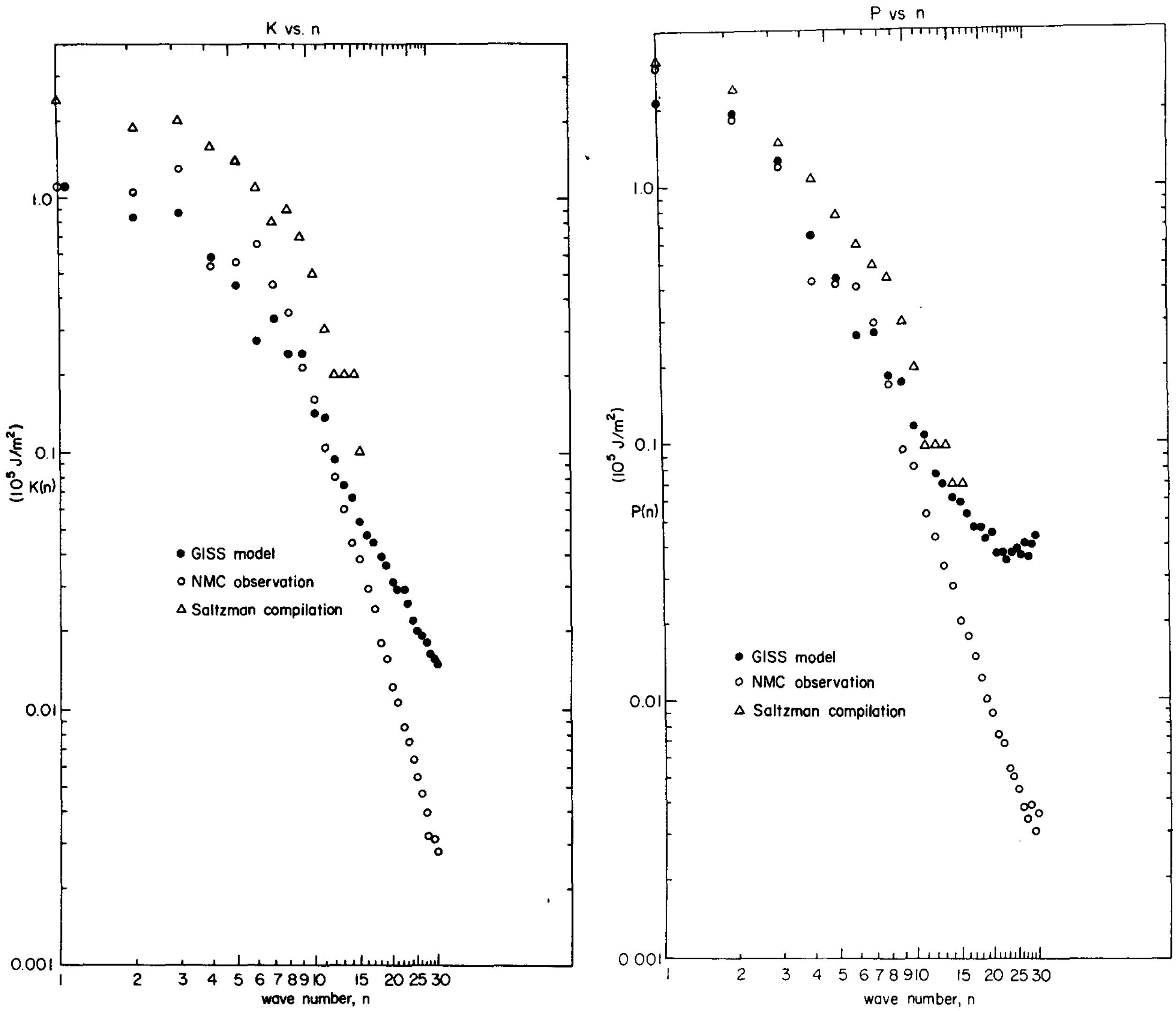

FIG. 8. Eddy kinetic energy and eddy available potential energy spectra vs wavenumber: (a) $K(n)$, (b) $P(n)$.

The flux of energy must be small in the inertial region corresponding to a -3 slope. Barros and Wiin-Nielsen (1974) define this flux as

$$\frac{\partial F}{\partial n}=C[K(m|n)],$$

where n is the wavenumber. By noting that

$$\int_0^{n_{\max}} dnC[K(m|n)]=0$$

we may choose the constant of integration. If we let $F(0)=0$, then

$$F(n)=\int_0^n dn'C[K(m|n')].$$

The results of this calculation are shown in Fig. 9 for the GISS model and NMC observations. The agreement is good with a near-zero flux in the inertial region. Similar results and the lack of an exact sum to zero (i.e., area under the curve equal to zero) were also obtained by Manabe *et al.* (1970). The residual flux may be due to the approximations inherent in finite differencing.

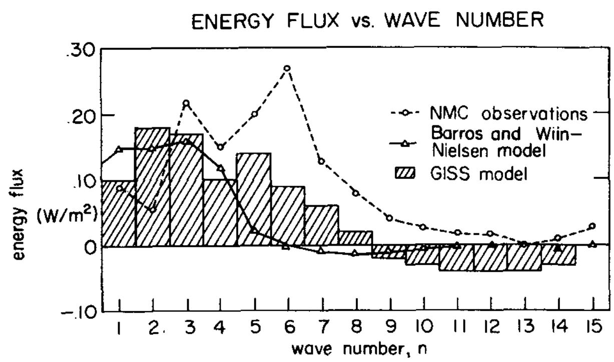

FIG. 9. Energy flux cascading through wavenumber n vs wavenumber. Barros and Wiin-Nielsen observations from Barros and Wiin-Nielsen (1974).

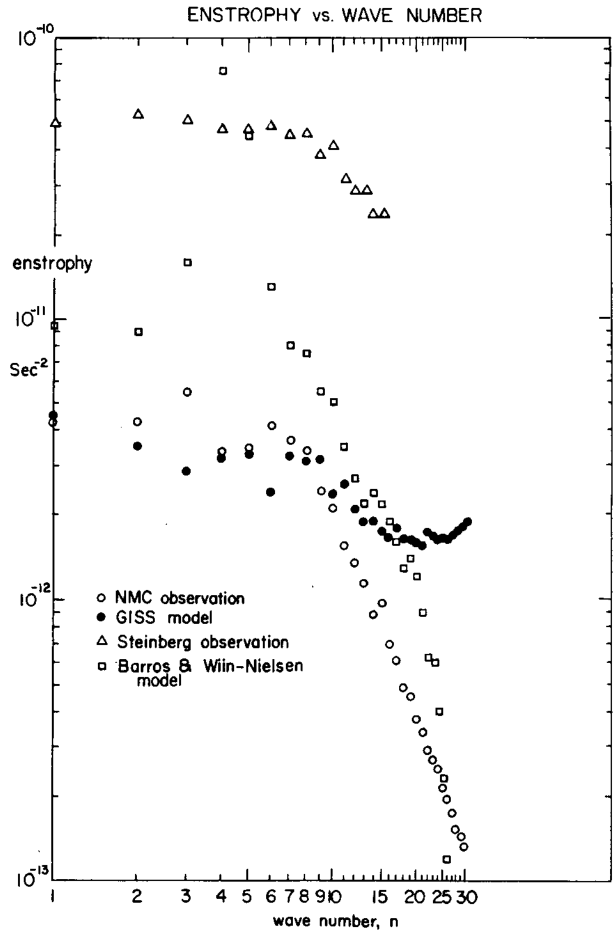

FIG. 10. Enstrophy vs wavenumber. Steinberg observations from Steinberg (1971). Barros and Wiin-Nielsen model data from Barros and Wiin-Nielson (1974).

c. Enstrophy

Enstrophy (mean squared vorticity) enters explicitly into both turbulence theory and Arakawa's numerical difference schemes. In turbulence theory the inertial subrange corresponds to a wavenumber region of constant enstrophy flux. In Arakawa's numerical difference scheme, enstrophy is explicitly conserved in the limit of non-divergent mass flux. Although enstrophy flux requires extensive additional calculations (Steinberg, 1971; Steinberg *et al.*, 1971), enstrophy itself is not difficult to calculate. Its precision is limited because of the need to difference two almost equal observed quantities.

Fig. 10 shows the enstrophy spectrum for the GISS model, NMC observations, Steinberg *et al.*'s (1971) observations, and Barros and Wiin-Nielsen's (1974) model. The inertial range slopes are comparable, and equal the kinetic energy slopes decreased by 2, a result derived in Steinberg (1971, Appendix C) for a 2-dimensional wavenumber. The absolute values differ substantially. The explanation is probably related to the excess magnitude found for the related analyses of Yang and Wiin-Nielsen discussed in Section 4a. The flattening in the GISS model at large wavenumbers probably indicates the generation of higher frequency waves as an artifact of the differencing needed to calculate enstrophy or difficulties with the effective viscosity.

d. Integrated energetics

Paper S makes comparison only with the annual cycle given in Oort (1964). In more recent work, Peixoto and Oort (1974) give a January energy cycle. This more recent study involved the space-time domain while the comparisons in paper S were made in the space domain. The difference involves defining $K(0)$ as the mean zonal motion (space domain) or as the mean zonal and temporal motion (space-time domain). In both cases the summed $K(n)$ are the difference between $K(0)$ and K_T, the total kinetic energy. Peixoto and Oort conclude that the differences for the conversion terms are not significant. Calculations of the energetics made in connection with paper S showed negligible differences for space and space-time values of $P(0)$, $P(n)$, $K(0)$ and $K(n)$. Figs. 11 a–d present the new Peixoto and Oort cycle, the spectrally summed

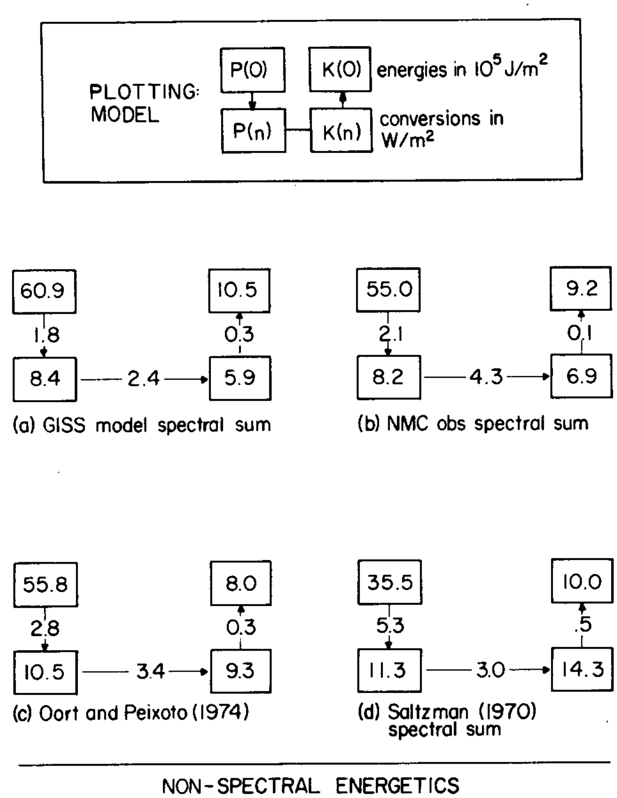

FIG. 11. Non-spectral energetics diagram. (a) GISS model for January 1973, integrated from 110 mb to the earth's surface for the Northern Hemisphere (levels 2 through 9 in Somerville *et al.* (1974). The non-zonal energies and conversions are summed over wavenumbers 1 through 30. (b) NMC observations. (c) Data from Oort and Peixoto (1974) for January. (d) Data from Saltzman (1970) for winter with non-zonal energies and conversions summed over wavenumbers 1 through 15. Diagrams (a), (b) and (d) are in the space domain; diagram (c) is in the space-time domain.

cycle implicit in Saltzman (1970), the spectrally summed cycle of the GISS model, and the spectrally summed cycle calculated from the NMC observational analysis. Our values of $P(0)$ and $P(n)$ are calculated on isobaric surfaces. Dutton and Johnson (1967) have argued that an error of up to a factor of 2 is possible as a result.

For $P(0)$ the results now show good agreement between Peixoto-Oort, the NMC January data, and the model. This removes the problem of comparing with annual and seasonal data as in paper S. As indicated previously, Saltzman's data for $K(n)$ are high. For $K(0)$ there is a general agreement among all four sources. The remaining energies and conversions are also in reasonable agreement except $C[P(0), P(n)]$ from Saltzman.

e. Spatial energetics

Peixoto and Oort have also presented spatial distributions of the various energies (Peixoto and Oort, 1974) and conversions (Oort and Peixoto, 1974).

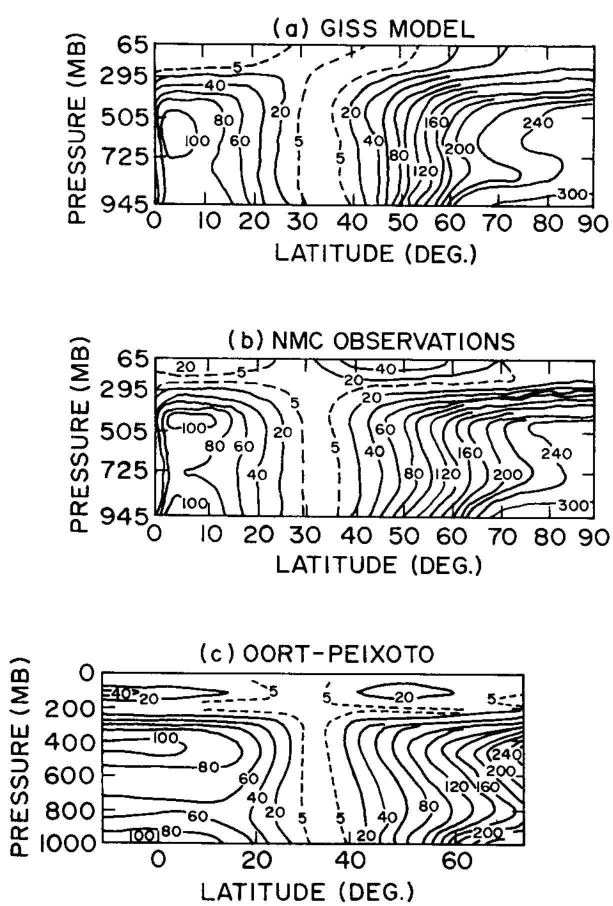

FIG. 12. (a) Spatial distribution of the zonal available potential energy $P(0)$ for the Northern Hemisphere, January 1973, from the GISS model. (b) NMC observations. (c) Northern Hemisphere and equatorial regions for January from Peixoto and Oort (1974). Units: 10^5 J/(m^2 bar).

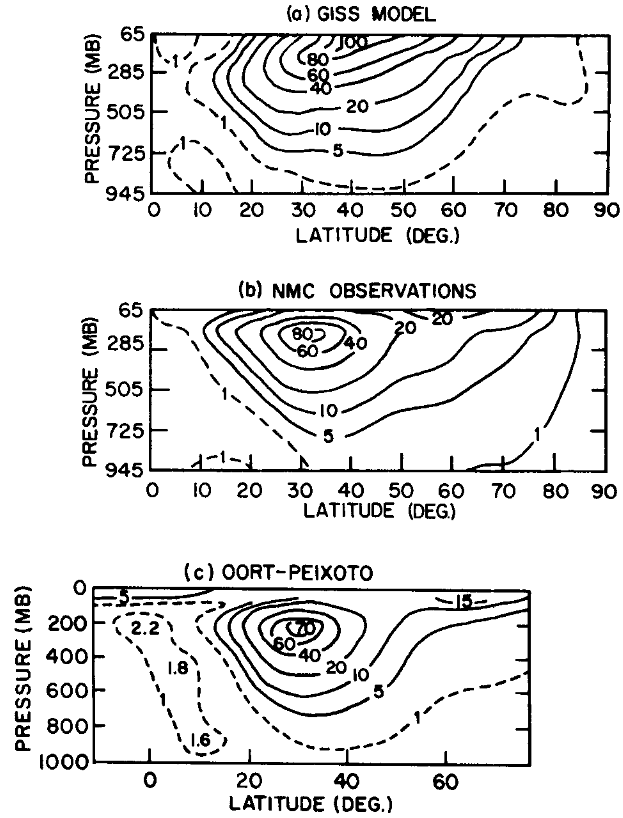

FIG. 13. (a) Spatial distribution of the zonal kinetic energy $K(0)$ for the Northern Hemisphere, January 1973, from the GISS model. (b) NMC observations. (c) Northern Hemisphere and equatorial regions for January from Peixoto and Oort (1974). Units: 10^5 J/(m^2 bar).

In general we find good agreement between their results, the GISS model, and NMC data as displayed in Figs. 12–17.

Fig. 12 shows $P(0)$. We find all three results contain peaks in the equatorial region and at sub-polar latitudes. The good equatorial agreement is an encouraging by-product of a global model. Fig. 13 shows $K(0)$. There is good quantitative agreement on the location, height and strength of the time-averaged jet stream. Its broadening in the model is evident, a defect to be noted again below.

The eddy terms are formed by summing over wavenumbers 1 to 30. Fig. 14 shows $P(n)$. The only strong feature is a near-surface peak in high latitudes, located correctly but with a larger peak value in the model. Fig. 15 shows $K(n)$. Hence there is significant disagreement, with both sets of observations agreeing, but with the model showing a weaker peak at the same level, displaced well northward.

Fig. 16 shows

$$\sum_{n=1}^{30} C[P(0),P(n)],$$

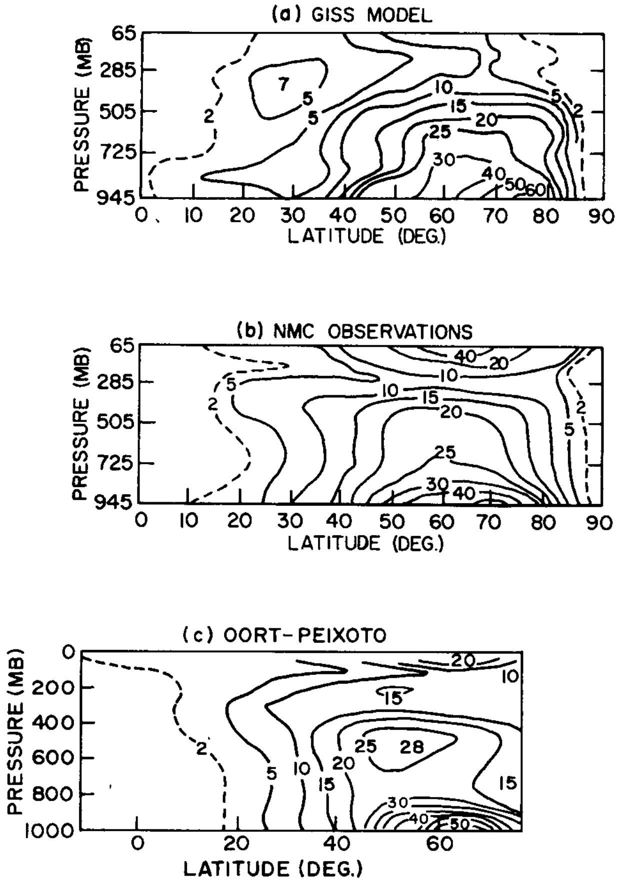

FIG. 14. (a) Spatial distribution of the eddy available potential energy $P(n)$ summed from wavenumbers 1 through 30. Data is for Northern Hemisphere, January 1973, for the GISS model. (b) NMC observations. (c) Eddy available potential energy from Peixoto and Oort (1974). Data are for Northern Hemisphere and equatorial regions for January. Their calculation is equivalent to a spectral sum over all wavenumbers. Units: 10^5 J/(m^2 bar).

the conversion to eddy available potential energy. The upper troposphere values are comparable but here the two observational data sets disagree on the existence of a near surface peak. In contrast, the corresponding term for kinetic energy conversion in Fig. 17,

$$\sum_{n=1}^{30} C[K(n),K(0)],$$

shows a most pronounced difference between model and observations. Both observational data sets show a characteristic conversion to the mean flow south of the jet and from the mean flow north of it. In the GISS model results the peak north of the jet is distinctly absent. Since this conversion term is proportional to $\partial v/\partial\phi$, the effects of a weak, diffuse jet stream is clearly shown.

f. Viscosity dependence

During the development of the model it was found that the general circulation depended sensitively on the kinematic viscosity used in the parameterization of vertical eddy transport of horizontal momentum. This dependence has been studied further in a subsequent paper (Stone *et al.*, 1974). They found that a large eddy viscosity (20 m^2 s^{-1}) improved the tropical flow but decreased the extratropical eddy motions to unrealistic values.

Figs. 18a, b present the $K(n)$ and $P(n)$ spectra from their case A (eddy viscosity = 0) and case B (eddy viscosity = 20 m^2 s^{-1}). These figures show that the eddy energies are reduced uniformly at all scales except for $n=3$ which is influenced by orography (Manabe and Terpstra, 1974) and $n=7$. The inertial range is still present with slopes for case A of -3.2 and case B of -2.9. Because of other changes the standard model (case *C* in Stone *et al.*, 1974) is not exactly comparable. However, we do note that the high viscosity run retains some but not all of the extraneous high frequency energy in $P(n)$ and enstrophy.

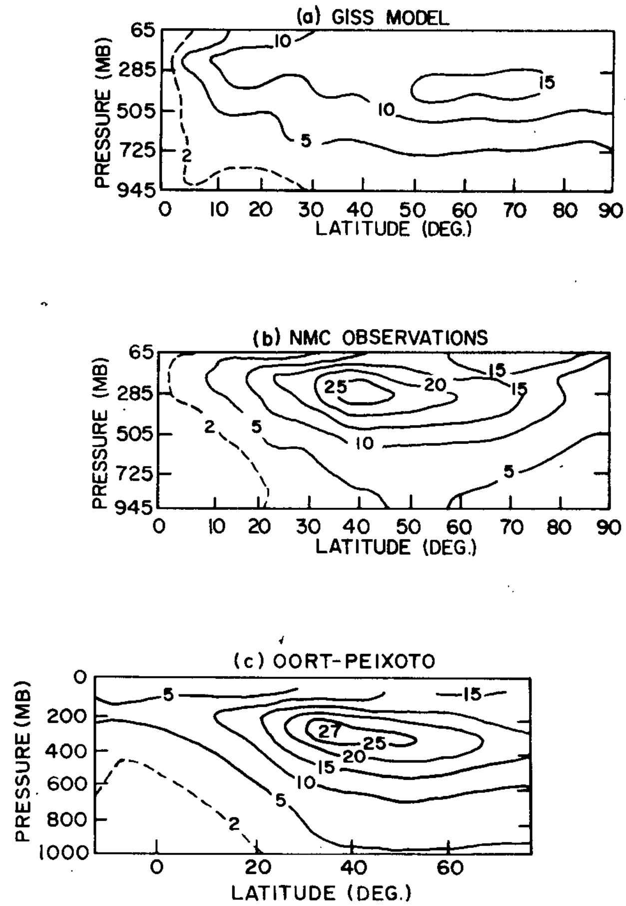

FIG. 15. (a) Spatial distribution of the eddy kinetic energy $K(n)$ summed from wavenumbers 1 through 30. Data are for Northern Hemisphere, January 1973, for the GISS model. (b) NMC observations. (c) Eddy kinetic energy from Peioxto and Oort (1974). Data are for Northern Hemisphere and equatorial regions for January. Their calculation is equivalent to a spectral sum over all wavenumbers. Units: 10^5 J/(m^2 bar).

5. Conclusions

Our analysis of the spectral energetics diagram for the GISS model and NMC observations of January 1973 leads to the following conclusions. Except for diffuse eddy kinetic energy, other larger-than-grid-scale processes have been correctly modeled. Specific examples are: 1) Significant nonlinear energy transfers were obtained in the wavenumber region 5–15 with a relatively coarse nominal resolution of 4° (latitude) by 5° (longitude). 2) The baroclinic conversion $C[P(n), K(n)]$ is large near the middle wavenumbers, 6–8, but does not show the sharp peaking of non-orographic models and observations. Further investigation is needed to resolve whether this is a real effect or an artifact of difficulties with ω dependent quantities. 3) The energetics of the model are internally consistent. For all n's except the first few, the residual of the inputs and outputs to $K(n)$ shows no systematic trend with n. The first few waves and especially $n=3$ have imbalances related to orography. 4) In all of these results, Saltzman's compilation seems to be based on analyses yielding energies which appear about 25% too large.

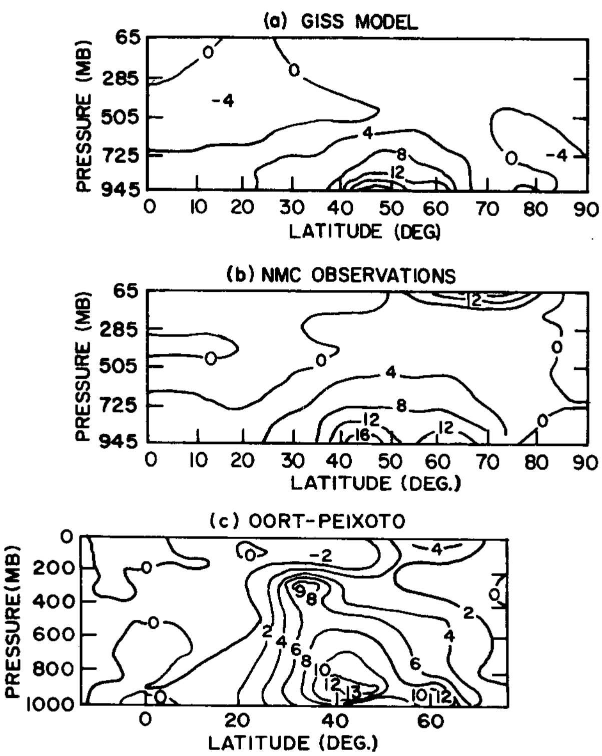

FIG. 16. (a) Spatial distribution of the conversion from zonal available potential energy to eddy available potential energy, $C[P(0), P(n)]$, summed from wavenumbers 1 through 30. Data are for Northern Hemisphere, January 1973, for the GISS model. (b) NMC observations. (c) Conversion term from Oort and Peixoto (1974). Data are for Northern Hemisphere and equatorial regions for January. Their calculation is equivalent to a spectral sum over all wavenumbers. Units: W/(m² bar).

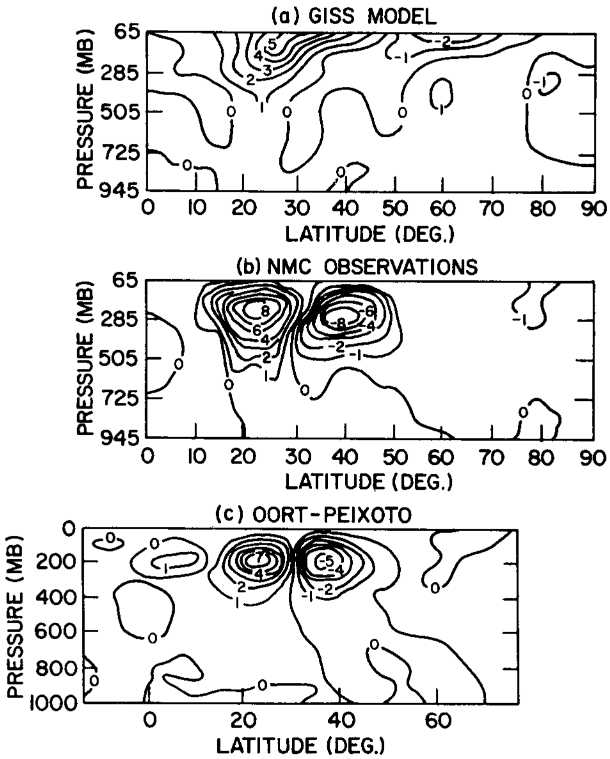

FIG. 17. (a) Spatial distribution of the conversion from eddy kinetic energy to zonal kinetic energy, $C[K(n), K(0)]$, summed from wavenumbers 1 through 30. Data is for Northern Hemisphere, January 1973, for the GISS model. (b) NMC observations. (c) Conversion term from Oort and Peixoto (1974). Data are for Northern Hemisphere and equatorial regions for January. Their calculation is equivalent to a spectral sum over all wavenumbers. Units: W/(m² bar).

Subgrid-scale processes are consistent with an inertial range characterized by zero energy flux. These data display simple power law behavior in $P(n)$, $K(n)$ and enstrophy in the range $n=8$ to 15. The necessary condition that the energy flux be very small was explicitly verified. Exact slopes must be treated with caution in view of the effects of smoothing and orography.

The model spatial energetics are in good agreement with both NMC observations for January 1973 and Peixoto and Oort's (1974) climatological January. The non-spectral energy diagram is now also in very good agreement. Our two areas of disagreement are in the sharpness of the jet stream and in the absence of the conversion $C[K(n), K(0)]$ north of it. We have also explicitly calculated the enstrophy. The model spectrum shape is comparable to observation but there is a significant difference in absolute magnitude. The excess values of both $P(n)$ and enstrophy for $n \gtrsim 25$ may indicate evidence of truncation problems for energy terms sensitive to differences. Continuing work on the effects of greater resolution, more accurate difference schemes, and improved model physics is underway to examine these problems.

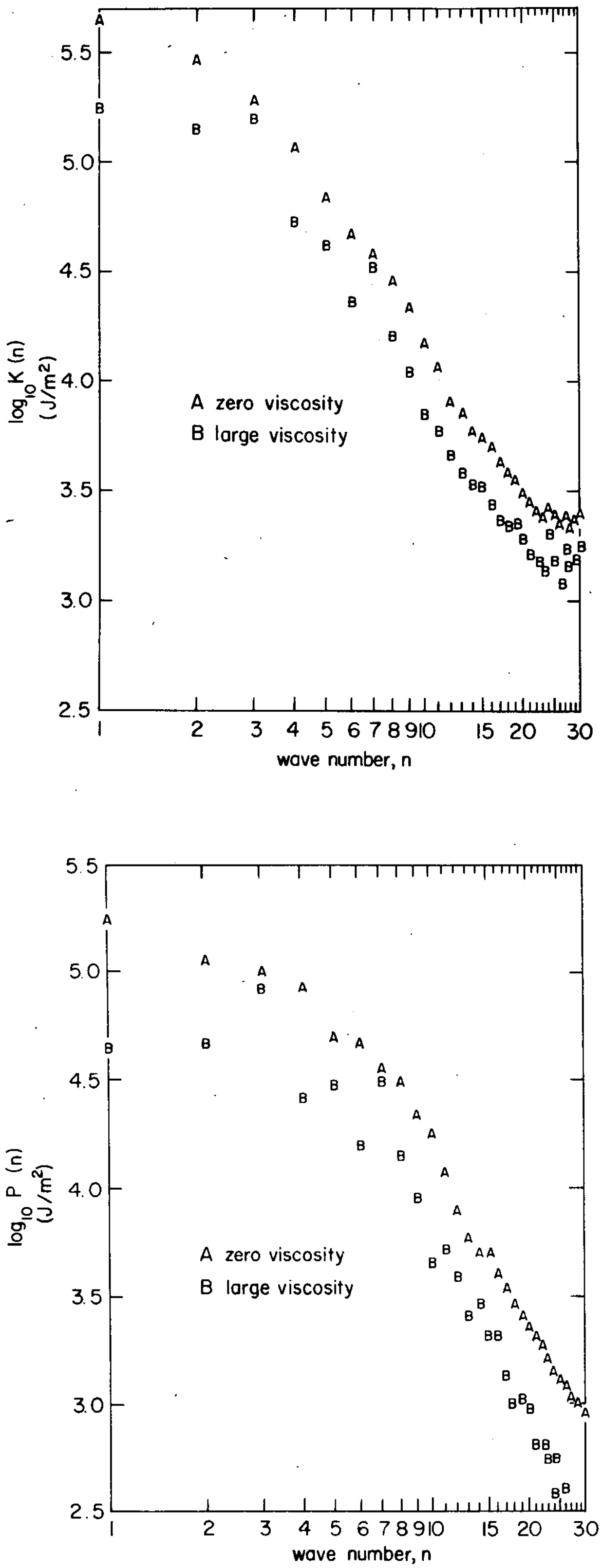

FIG. 18. (a) Eddy kinetic energy and (b) eddy available potential energy for the zero viscosity and large viscosity cases of Stone *et al.* (1974).

Acknowledgments. I am grateful to Richard Somerville and Peter Stone for encouragement and many helpful comments. William Quirk was equally helpful, and, in addition, provided the basic diagnostic programs upon which the spectral analysis was superimposed. Abe Seidman provided some useful suggestions on spectral analysis.

APPENDIX A

Bias-Free Spectra in Mountainous Regions

For clarity let us work with discrete Fourier series and an explicit sine, cosine formulation. Let $h(x)$ be an arbitrary function whose value is known at $2N$ points, x_i, $i=0$ to $2N-1$. Then $h(x)$ may be represented by a Fourier series as

$$h(x)=\sum_{n=0}^{N-1}(A_n \cos nx+B_n \sin nx).$$

For simplicity of notation we will not separate out A^0 and will include B_0 which is identically 0. The standard procedure for obtaining the A_n is to multiply through by $\cos mx_i$ and sum both sides over all the points x_i:

$$\sum_{i=0}^{2N-1} \cos mx_i \cdot h(x_i)$$

$$=\sum_{i=0}^{2N-1}\sum_{n=0}^{N-1}(A_n \cos nx_i+B_n \sin nx_i)\cdot \cos mx_i. \quad (1)$$

Interchanging summations on the right hand side and using

$$\sum_{i=0}^{2N-1} \cos nx_i \cos mx_i=\begin{cases} N, & n=m, \neq 0 \\ 0, & n\neq m \end{cases}$$

$$\sum_{i=0}^{2N-1} \sin nx_i \cos mx_i=0$$

yields

$$\sum_{i=0}^{2N-1} \cos mx_i \cdot h(x_i)=A_m N,$$

which yields A_m without difficulty. A similar procedure yields B_m.

Let us now repeat the process but omit from the left-hand side of (1) the term for some $i=j$ at which point the function $h(x_j)$ may be unknown. Then we obtain

$$\sum_{i=0,\neq j}^{2N-1} \cos mx_i \cdot h(x_i)$$

$$=\sum_{i=0}^{2N-1}\sum_{n=0}^{N-1}(A_n \cos nx_i+B_n \sin nx_i)\cdot \cos mx_i$$

$$-\sum_{n=0}^{N-1}(A_n \cos nx_j+B_n \sin nx_j)\cdot \cos mx_j$$

or

$$\sum_{i=0,\neq j}^{2N-1} \cos mx_i \cdot h(x_i) = A_m \cdot N - \sum_{n=0}^{N-1} (A_n \cos nx_j + B_n \sin nx_j) \cdot \cos mx_j, \quad (2)$$

with a corresponding equation for the sine terms

$$\sum_{i=0,\neq j}^{2N-1} \sin mx_i \cdot h(x_i) = B_m \cdot N - \sum_{n=0}^{N-1} (A_n \cos nx_j + B_n \sin nx_j) \cdot \sin mx_j. \quad (3)$$

To simplify notation we let $\mathbf{C}$ be a $2N$ component vector defined as

$$\mathbf{C} = \begin{bmatrix} A_0 \\ \vdots \\ A_{N-1} \\ \cdot \\ B_0 \\ \vdots \\ B_{N-1} \end{bmatrix},$$

and $\mathbf{H}(\overline{x_j})$ be a $2N$ component vector consisting of the elements

$$H_m(\overline{x_j}) = \sum_{i=0,\neq j}^{2N-1} \cos mx_i \cdot h(x_i), \qquad m=0 \text{ to } N-1,$$

$$H_m(\overline{x_j}) = \sum_{i=0,\neq j}^{2N-1} \sin(m-N)x_i \cdot h(x_i), \quad m=N \text{ to } 2N-1,$$

where the notation $H(\overline{x_j})$ implies that it is not a function of x_j; and $T_{mn}(x_j)$ be a square matrix with row index m and column index n

$$\begin{array}{c|c} & \begin{array}{cc} n=0\cdots N-1 & N\cdots 2N-1 \end{array} \\ \begin{array}{c} m=0 \\ \vdots \\ N-1 \\ N \\ \vdots \\ 2N-1 \end{array} & \left[\begin{array}{c|c} \cos nx_j \cos mx_j & \sin(n-N)x_j \cos mx_j \\ \hline \cos nx_j \sin(m-N)x_j & \sin(n-N)x_j \sin(m-N)x_j \end{array}\right]. \end{array}$$

Then Eqs. (2) and (3) may be rewritten in the combined form

$$\mathbf{H}(\overline{x_j}) = N\mathbf{C} - T(x_j)\mathbf{C} = [N - T(x_j)]\mathbf{C},$$

or

$$\mathbf{C} = [N - T(x_j)]^{-1}\mathbf{H}(\overline{x_j}).$$

The inversion of this matrix gives the desired bias-free solution for the Fourier coefficients $\mathbf{C}$. It is bias-free in the sense that no arbitrary assumptions have been made about the values of the function h at the point x_j. Furthermore, the procedure is clearly generalizable to more than one missing point:

$$\mathbf{C} = (N - T(x_j) - T(x_k)\cdots)^{-1}\mathbf{H}(\overline{x_j}, \overline{x_k}, \cdots).$$

For a small number of points missing the matrix is likely to be well-conditioned. For a large number of points missing the matrix probably becomes ill-conditioned in analogy to the situation found by Julian and Cline (1974) for unequal station spacing.

REFERENCES

Arakawa, A., 1966: Computational design for long-term numerical integration of the equations of fluid motion: Two dimensional incompressible flow. Part I. *J. Comput. Phys.*, **1**, 119–143.

——, 1970: Numerical simulation of large-scale atmospheric motions. *Numerical Solution of Field Problems in Continuum Physics*, Providence, R. I., Amer. Math. Soc., 24–40.

——, 1972: Design of the UCLA atmospheric general circulation model. Tech. Rept. No. 7, Dept. of Meteorology, University of California at Los Angeles.

Baer, F., 1972: An alternate scale representation of atmospheric energy spectra. *J. Atmos. Sci.*, **29**, 649–664.

——, 1973: Spectral fidelity of gappy data. *Bull. Amer. Meteor. Soc.*, **54**, 748 [abstract].

Barros, V. R., and A. Wiin-Nielsen, 1974: On quasi-geostrophic turbulence: A numerical experiment. *J. Atmos. Sci.*, **31**, 609–621.

Charney, J. G., 1971: Geostrophic turbulence. *J. Atmos. Sci.*, **28**, 1087–1095.

Cooley, J. W., and J. W. Tukey, 1965: An algorithm for the machine calculation of Fourier series. *Math. Comput.*, **19**, 297–301.

Dutton, J. A., and D. R. Johnson, 1967: The theory of available potential energy and a variational approach to atmospheric energetics. *Advances in Geophysics*, Vol. 12, New York, Academic Press, 333–436.

Flattery, T. W., 1971: Spectral models for global analysis and forecasting. *Automated Weather Support—Proceedings of the 6th AWS Technical Exchange Conference, U. S. Naval Academy, 21–24 September 1970, 42–54.* [Available from Defense Documentation Center, Cameron Station, Alexandria, Va. 22314 as Air Weather Service Technical Report 242, AD-724093.]

Julian, P. R., and A. K. Cline, 1974: The direct estimation of spatial wavenumber spectra of atmospheric variables. *J. Atmos. Sci.*, **31**, 1526–1539.

——, W. M. Washingron, L. Hembree and C. Ridley, 1970: On the spectral distribution of large-scale atmospheric kinetic energy. *J. Atmos. Sci.*, **27**, 376–387.

Kasahara, A., and W. M. Washington, 1967: NCAR global general circulation model of the atmosphere. *Mon. Wea. Rev.*, **95**, 389–402.

—— and ——, 1971: General circulation experiments with a six-layer NCAR model, including orography, cloudiness and surface temperature calculations. *J. Atmos. Sci.*, **28**, 657–701.

Kraichnan, R. H., 1967: Inertial ranges in two-dimensional turbulence. *Phys. Fluids*, **10**, 1417–1423.

Kuo, H.-L., 1952: Three-dimensional disturbances in a baroclinic zonal current. *J. Meteor.*, **9**, 260–278.

Leith, C. E., 1968: Diffusion approximation for two-dimensional turbulence. *Phys. Fluids*, **11**, 671–673.

——, 1971: Atmospheric predictability and two-dimensional turbulence. *J. Atmos. Sci.*, **28**, 145–161.

Lilly, D. K., 1972: Numerical simulation studies of two-dimensional turbulence. *Geophys. Fluid Dyn.*, **3**, 289–319.

Lorenz, E. N., 1955: Available potential energy and the maintenance of the general circulation. *Tellus*, **7**, 157–167.

——, 1967: The nature and theory of the general circulation of the atmosphere. WMO Publ. 218-TP-115, Geneva, 161 pp.

Manabe, S., J. Smagorinsky and R. F. Strickler, 1965: Simulated climatology of a general circulation model with a hydrologic cycle. *Mon. Wea. Rev.*, **92**, 769–798.

——, J. Smagorinsky, J. L. Holloway, Jr. and H. M. Stone, 1970: Simulated climatology of a general circulation model with a hydrologic cycle. III. Effects of increased horizontal computational resolution. *Mon. Wea. Rev.*, **98**, 175–212.

——, and T. B. Terpstra, 1974: The effects of mountains on the general circulation of the atmosphere as identified by numerical experiments. *J. Atmos. Sci.*, **31**, 3–42.

Oort, A. H., 1964: On estimates of the atmospheric energy cycle. *Mon. Wea. Rev.*, **92**, 483–493.

——, and J. P. Peixoto, 1974: The annual cycle of the energetics of the atmosphere on a planetary scale. *J. Geophys. Res.*, **79**, 2705–2719.

Peixoto, J. P., and A. H. Oort, 1974: The annual distribution of atmospheric energy on a planetary scale. *J. Geophys. Res.*, **79**, 2149–2159.

Saltzman, B., 1957: Equations governing the energies of the larger scales of atmospheric turbulence in the domain of wave number. *J. Meteor.*, **14**, 513–523.

——, 1970: Large scale atmospheric energetics in the wavenumber domain. *Rev. Geophys. Space Phys.*, **8**, 289–302.

——, and A. Fleisher, 1961: Further statistics on modes of release of available potential energy. *J. Geophys. Res.*, **66**, 2271–2273.

Shuman, F. G., and J. B. Hovermale, 1968: An operational six-layer primitive equation model. *J. Appl. Meteor.*, **7**, 525–547.

Smagorinsky, J., S. Manabe and J. L. Holloway, Jr., 1965: Numerical results from a nine-level general circulation model of the atmosphere. *Mon. Wea. Rev.*, **93**, 727–768.

Somerville, R. C. J., P. H. Stone, M. Halem, J. E. Hansen, J. S. Hogan, L. M. Druyan, G. Russell, A. A. Lacis, W. J. Quirk and J. Tenenbaum, 1974: The GISS model of the global atmosphere. *J. Atmos. Sci.*, **31**, 84–117.

Starr, V. P., 1968: *Physics of Negative Viscosity Phenomena*. New York, McGraw-Hill, 256 pp.

Steinberg, H. L., 1971: On power laws and nonlinear cascades in large-scale atmospheric flow. Tech. Rept. 002630-4-T, The University of Michigan, Ann Arbor, 143 pp.

——, A. Wiin-Nielsen and C.-H. Yang, 1971: On nonlinear cascades in large-scale atmospheric flow. *J. Geophys. Res.*, **76**, 8629–8640.

Stone, P. H., W. J. Quirk and R. C. J. Somerville, 1974: The effect of small-scale vertical mixing of horizontal momentum in a general circulation model. *Mon. Wea. Rev.*, **102**, 765–771.

Wallace, J. M., 1971: Spectral studies of tropospheric wave disturbances in the tropical Western Pacific. *Rev. Geophys. Space Phys.*, **9**, 557–612.

Wellck, R. E., A. Kasahara, W. M. Washington and G. De Santo, 1971: Effect of horizontal resolution in a finite difference model of the general circulation. *Mon. Wea. Rev.*, **99**, 673–683.

Wiin-Nielsen, A., 1964: Some new observational studies of energy and energy transformations in the atmosphere. WMO Tech. Note 66, Geneva, 177–202.

——, 1967: On the annual variation and spectral distribution of atmospheric energy. *Tellus*, **19**, 540–559.

Yang, C.-H., 1967: Nonlinear aspects of the large-scale motion in the atmosphere. Tech. Rept. 08759-1-T, The University of Michigan, Ann Arbor, 173 pp.